RSC Advances

ROYAL SOCIETY OF CHEMISTRY

www.rsc.org/advances

Journal Name

ARTICLE

Synergistic Effects of Halogen Bond and π-π Interactions in Thiophene-based Building Blocks

Received 00th January 20xx,
Accepted 00th January 20xx

DOI: 10.1039/x0xx00000x

www.rsc.org/

Jamey Wilson, Jon Steven Dal Williams, Chesney Petkovsek, Peyton Reves, Jonah W. Jurss, Nathan I. Hammer, Gregory S. Tschumper, Davita L. Watkins*

Although recognized as a significant force in crystal engineering, halogen bonding (XB) has been scarcely investigated in "bottom-up" approaches towards organic electronics. We report, herein, the use of a thiophene-based building block, pyridyl-thiophene (Pyr-T), to achieve an assembly driven by XB and π-π stacking interactions with that of iodopentafluorobenzene (IPFB). Spectroscopic and thermal analysis of the co-crystal provide indirect evidence of the assembly. The combined effect of XB and π-π stacking are confirmed experimentally via X-ray crystallography. Density functional theory (DFT) computations support experimental observations. The results of the study speak to the use of halogen bond driven self-assembly in organic electronic device application.

Introduction

Organic semiconducting devices have received enormous attention as low cost and flexible alternatives to silicon-based technologies.[1, 2] Studies within the field of organic electronics have emerged linking its progression towards "bottom-up" approaches. The basis of these studies is aimed at understanding the molecular assembly of complex π-conjugated systems as a means to increase device efficiency.[3-6] It has been demonstrated that the synergistic action of non-covalent interactions such as hydrogen bonding (HB) and π-π stacking in thiophene-based donors can induce well-defined solid state packing between molecules.[7, 8] The strategic design of these π-conjugated oligomers, equipped with self-guided domains, can increase overall device performance and stability.

Although recognized as a significant force in improving the packing of many halogen-containing organic compounds,[9-12] halogen bonding (XB) has been scarcely investigated within "bottom-up" approaches towards organic devices.[13-16] Halogen bonds, analogues of hydrogen bonds, are non-covalent interactions between Lewis acidic halogen atoms and electron-pair-donating heteroatoms.[17] The phenomenon is explained by the presence of a region of positive electrostatic potential (i.e., σ-hole) on the outermost surface of the halogen atom.[18] This area of electron deficiency affords a highly directional interaction with electron donating heteroatoms.

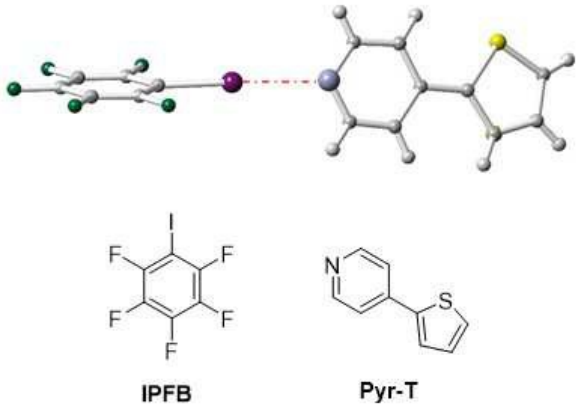

Figure 1. Top image: X-ray structural analysis of the complex of halogen bond donor and acceptor. Selected bond distances [Å] between nitrogen and halogen is 2.76 Å (red dotted line). Bottom image: Molecular structure of **Pyr-T** and **IPFB**

Such an effect can be greatly beneficial in organizing π-conjugated molecules that are potentially relevant to organic electronics applications.

As a result, well-defined assemblies can be engineered by exploiting the interactions between XB and π stacking in thiophene-based building blocks.

Herein, we investigate the halogen bond driven assembly between pyridyl thiophene (**Pyr-T**)—a π-conjugated building block equipped with a self-assembling domain—and iodopentafluorobenzene (**IPFB**) (Figure 1). The truncated version of a pyridyl-capped oligothiophene (e.g., **Pyr-T**) is employed to provide a fundamental understanding and design guidelines for the synthesis and characterization of more complex molecular assemblies. It was chosen as the XB-acceptor (i.e., pyridyl N as the electron donor) because it can be easily integrated into the oligomeric framework of any π-

Department of Chemistry and Biochemistry, University of Mississippi, University, MS 38677-1848. Email: dwatkins@olemiss.edu

† Electronic Supplementary Information (ESI) available: [details of any supplementary information available should be included here]. See DOI: 10.1039/x0xx00000x

‡ The manuscript was written through contributions of all authors. All authors have given approval to the final version of the manuscript

conjugated system via palladium-catalyzed cross coupling. The XB-donor, **IPFB**, was selected as the electron acceptor as the fluoro substituents provide an inductive effect which increases σ-hole bonding.[19-21] The presence of XB and π-π stacking was confirmed experimentally via X-ray crystallography, NMR, and Raman spectroscopy. Further analysis via density functional theory (DFT) computations supports experimental observations and reveals that XB and π-stacking provide the dominant energetics in the observed assembly.

Experimental section

General remarks

Reagents and solvents were purchased from commercial sources and used without further purification unless otherwise specified. ^{1}H and ^{13}C NMR spectra were recorded on a Bruker Avance-300 (300 [75] MHz), Bruker Avance DRX-500 (500 [125] MHz) spectrometer and are reported in ppm using the solvent as an internal standard ($CDCl_3$ at 7.26 ppm). Additional synthetic details, Raman spectroscopy data, summary of theoretical calculations, structural figures, TGA plots, and X-ray crystallographic tables containing bond distances and angles can be found in the ESI.

X-ray crystallography

Crystal evaluation and data collection were performed on a Bruker APEX II diffractometer with Mo Kα (λ = 0.71073 Å) radiation. Reflections were indexed by an automated indexing routine built in the APEXII program suite. The solution and refinement was carried out in Olex^2 version 1.2 using the program SHELXTL. Non-hydrogen atoms were refined with anisotropic thermal parameters while hydrogen atoms were introduced at calculated positions based on their carrier/parent atoms. Crystal data and structure refinement parameters for all compounds are given in Tables S1. The single crystal X-ray structure of the co-crystal CCDC number is 1410980.

Crystal data. Crystal Data for $C_{15}H_7F_5INS$ (FW = 455.18 g/mol): mono-clinic, space group $P2_{1/n}$ (no. 14), a = 8.7694(5) Å, b = 7.5097(4) Å, c = 22.9574(13) Å, β = 91.757(3)°, V = 1511.16(15) Å3, Z = 4, T = 100(2) K, Mo-Kα = 0.71073 Å, μ = 2.307 mm-1, D_{calc} = 2.001 g/cm^3, 26339 reflections measured (3.54° ≤ 2Θ ≤ 52.98°), 3130 unique (R_{int} = 0.0266), which were used in all calculations. The final R_1 was 0.0158 ($I > 2\sigma(I)$) and wR_2 was 0.0377 (all data).

Theoretical methods

The Gaussian 09 software package was employed to calculate the energies of interaction and vibrational frequencies as well as the corresponding Raman intensities. The B3LYP[22-24] and M06-2X[25] global hybrid density functional method was used in conjunction with the following triple-zeta basis sets: 6-311+G(2*df*,2*pd*), def2-TZVPD, and aug-cc-pVTZ.

Raman spectroscopy

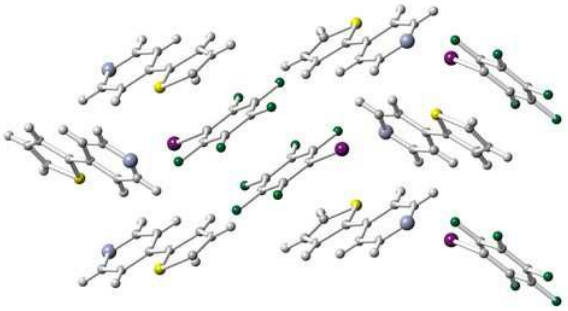

Figure 2. Fragment of the packing diagram along the *a*-axis conveying the presence of both XB and π-interactions

Raman spectra of the monomer and co-crystal were obtained by using methods similar to those previously reported.[26] A LabView-controlled Jobin-Yvon Ramanor HG2-S Raman spectrometer was employed. A 647.1 nm line of a SpectraPhysics Kr+/Ar+ laser was used as the excitation source. A photomultiplier tube was used as the detector for the setup. The solid crystals were placed onto a microscope slide and positoned on the microscope stage in the path of the laser. The crystals were scanned from 20-2000 cm^{-1} four times at a speed of 2 cm^{-1} per second. The experimental data gathered from Raman spectroscopic analysis was graphed using the IGOR Pro graphing program.

Thermogravimetric Analysis

Measurements were performed on Seiko Instruments TG/DTA 6200 (platinum pan, room temperature to 600 °C, ramp rate of 20 °C min^{-1} under nitrogen atmosphere) and analysed on TG/DTA Highway Conversion Software.

Results and discussion

Pyr-T was synthesized according to a previously published procedure.[27] Experimental studies to identify the signature of XB began with solution-based ^{1}H and ^{13}C NMR (Figure S1 and S2). NMR spectra of chemical shifts are commonly employed to afford insight into the strength of the bonds.

Spectra of a 1:1 mixture of **IPFB** and **Pyr-T** are taken in a halogen bond promoting solvent (i.e., 150 mM; toluene-d_8) and compared to a neat solution of **Pyr-T**.[28] As the lone pairs on the pyridyl nitrogen interact with the region of positive electrostatic potential on the iodine in **IPFB**, the electronegativity of the nitrogen decreases. The peaks corresponding to the proton and carbon nuclei ortho (toluene-d_8: δH 8.63 ppm, δC 151.3 ppm) to the nitrogen atom become more shielded. However, chemical shifts with changes less than 1 ppm indicate that weak intermolecular interactions between the solvent and solute are screening the effects of XB.

Co-crystals of **Pyr-T** and **IPFB** were prepared at a 1:1 ratio by dissolving **Pyr-T** in tetrahydrofuran with **IPFB** in borosilicate glass vials. The resulting mixture was ultrasonicated for 10

minutes. The open vials were contained in a secondary vial containing *n*-hexane. The solvent was allowed to evaporate at -20 °C for 14 days until the formation of crystals. Confirmation of co-crystallization was observed through a ~26 °C difference in melting point between the co-crystal (66 °C) and the Pyr-T monomer (92 °C).[29, 30] Single crystal X-ray analysis provides detail about the 1:1 assembly of **Pyr-T** and **IPFB** (Figure 2). Antiparallel arrangement of the donor-acceptor pairs in the crystal are indicated by the monoclinic space group, $P2_1/n$. This arrangement is preferential as the high molecular dipole moment of each molecule is cancelled and electrostatic repulsion is avoided. In analysing the solid state assembly, the strength of the halogen bond is associated with the distance and angle between the donor and acceptor atoms. Stronger halogen bonds can possess a nearly linear geometry between the electron donor and carbon-halogen acceptor (e.g., N···X—C) and distances 20 to 30 % shorter than the sum of the corresponding van der Waals radii of the complexing atoms.[31, 32] The N···X—C angle in the co-crystal is 178.8°. The N···I distance is 2.76 Å, which corresponds to a 22 % shortening relative to the total van der Waals radii of nitrogen and iodine.

Observed among the two end-to-end XB interactions are important lateral intermolecular contacts between adjacent molecules. When viewed along the *a*-axis (Figure 2), adjacent molecules are in contact through C—H···F interactions with an average distance of 2.70 Å. The negative charge distribution surrounding the fluorine atom affords this hydrogen-fluorine relationship. The interaction occurs between the meta hydrogens of the pyridyl ring and the ortho fluorines of the neighboring iodopentafluorobenzene. **Pyr-T** molecules are arranged in an edge-to-face orientation with opposing molecular dipoles. The centroid to centroid distance between the fluoroaromatic and thiophene ring of **Pyr-T** is approximately 3.68 Å, indicative of π-π stacking. The interaction is due to the interplay of electron deficiency in the fluorinated ring and electron-richness of the thiophene. In addition, the fluoroaromatic rings are arranged in an offset π-π stacked orientation in which the distance between the two centroids is 4.43 Å. These additional intermolecular interactions contribute to the stability of the assembly.

DFT computations were employed to investigate the relative strengths of the interactions forming the assembly. Analysis began with optimization of the **Pyr-T** monomer. According to B3LYP[22-24] and M06-2X[25] computations with sufficiently flexible triple-zeta basis sets (6-311+G(2*df*,2*pd*)[33], def2-TZVPD[34] and aug-cc-pVTZ[35-37]), the torsional angle of the carbon-sulfur bond relative to the pyridine ring-plane is roughly ±20° (Figure S3) indicating that an isolated **Pyr-T** monomer may be slightly non-planar. However, the perfectly planar structure is essentially isoenergetic (within 0.2 kcal/mol). Even though this planar structure is a transition state according to all DFT computations, the non-covalent contacts present in the crystal structure can certainly overcome this small energy difference and stabilize the planar conformation of **Pyr-T**. Consequently, the 1:1 assembly (or dimer) between **IPFB** and **Pyr-T** was examined in both a quasi co-planar orientation with C_1 symmetry and perpendicular

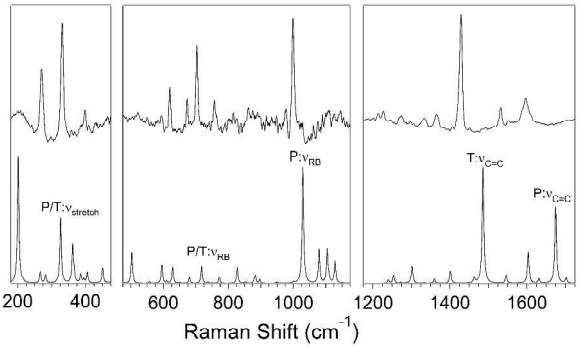

Figure 3. Comparison of the experimental (top) and theoretical using the M06-2X/aug-cc-pVDZ method and basis set combination (bottom) Raman spectra of **Pyr-T** within the co-crystal.

arrangement with C_s symmetry (Figure S4). The electronic energies of these two optimized dimer structures differ by less than 0.3 kcal/mol. The higher-energy perpendicular C_s structure is a transition state for rotation about the XB, which indicates that it is essentially a barrierless process. The M06-2X interaction energies of the nearest-neighbor pairwise contacts (Figure S5) observed in the crystal structure are summarized in Table S1. These results clearly show that the XB interaction and π-π stacking between **IPFB** and **Pyr-T** molecules are quite significant and of similar magnitude (roughly 8± 1 kcal/mol). The interaction energies for the other contacts between **IPFB** and **Pyr-T** are far smaller (*ca*. 1 kcal/mol). The only other appreciable interactions arise from π-π stacking between neighboring **IPFB** units (*ca*. 6 kcal/mol) and a face-to-edge contact between two **Pyr-T** fragments (*ca*. 4 kcal/mol). The results strongly suggest XB and π-π stacking provide the dominant forces driving the assembly of this system.

Additional evidence of XB is confirmed via Raman spectroscopy.[38] Analysis of the experimental Raman spectra of the **Pyr-T** monomer and the co-crystal was complicated by the presence of an emissive background. The emission is attributed to intramolecular charge transfer between the thiophene donor portion of the molecule and acceptor group, pyridine.[39] Typically, supramolecular assemblies resulting from XB afford blue shifts in the bands of the Lewis base and red shifts for the halogen containing molecule.[40] Comparison of the experimental Raman spectra indicated small blue shifts in the modes of the **Pyr-T** in the co-crystal (Table S2, Figure S6).

Collectively, experimental Raman features agree very well with theoretical predictions. Comparisons of experimental and theoretical Raman spectra of **Pyr-T** in the co-crystal using additional and different levels of theory are included in the SI (Figures S7-S12). Prominent features in the experimental spectrum include the stretch of the bond between the pyridyl and thiophene groups at 330 cm^{-1} and the concurrent ring-breathing mode of both pyridyl and thiophene at 703 cm^{-1}. Additional features of interest include the pyridyl ring breathing mode at 1000 cm^{-1} and the carbon-carbon double bond stretches of thiophene and pyridyl present at 1428 cm^{-1} and 1598 cm^{-1}, respectively. The magnitude of the vibrational

energy shifts are difficult to attribute directly to XB interactions. Despite this difference, many experimental characteristics are recovered by theory (Figure 3).

Relevant towards further applications in electronic devices is the thermal stability of the XB assembly. The thermal properties of the co-crystal compared to the monomer were examined using themogravimetric analysis (TGA). The thermal curve (Figure S7) for the co-crystal reveals a dual step decomposition pattern in which the initial decomposition is within 3 °C of that observed for **Pyr-T**. The co-crystal decomposes at 120 and 183 °C. The weight loss is higher than the decomposition temperature of the pure monomer. It is believed to be due to dissociation and possible sublimation of the **Pyr-T** prior to decomposition of the co-crystal as continuous weight losses above 100 °C were observed, which indicate the absence of solvent molecules in the crystal lattice.

Conclusions

In summary, we describe the use of a thiophene-based building block to achieve a supramolecular assembly driven by XB. Spectroscopic and thermal analysis affords evidence of XB between of **Pyr-T** and **IPFB**. X-ray crystallography and theoretical data of the co-crystal indicates that intermolecular interactions—specifically XB and π-stacking—contribute to the formation of the assembly. The results of the study speak to the use of XB molecules in organic electronic device application. Incorporation of the truncated model into more complex oligomers is currently underway.

Acknowledgements

D.L.W. appreciates financial support of this work from Oak Ridge Associated Universities through the Ralph E. Powe Award and the National Science Foundation, MRI; CHE-1338056. The computational work is supported by the Mississippi Center for Supercomputing Research and the National Science Foundation under Grant Numbers CHE-1338056 (G.S.T.). G.S.T and N.I.H. acknowledge NSF EPSCoR support under grant no. EPS-0903787 and N.I.H also acknowledges CHE-0955550 for support of the spectroscopic work. J.W.J. and D.L.W. thank the University of Mississippi for Laboratory Start-up Funds. Special appreciation to Dr. Amal Dass and colleagues for initial crystallographic data.

Notes and references

1 A. Mishra and P. Bäuerle, *Angew. Chem. Int. Ed.*, 2012, **51**, 2020-2067.
2 V. Coropceanu, H. Li, P. Winget, L. Zhu and J.-L. Brédas, *Annu. Rev. Mater. Res.*, 2013, **43**, 63-87.
3 S. J. Kang, S. Ahn, J. B. Kim, C. Schenck, A. M. Hiszpanski, S. Oh, T. Schiros, Y.-L. Loo and C. Nuckolls, *J. Am. Chem. Soc.*, 2013, **135**, 2207-2212.
4 A. S. Tayi, A. Kaeser, M. Matsumoto, T. Aida and S. I. Stupp, *Nat Chem*, 2015, **7**, 281-294.
5 E. D. Głowacki, L. Leonat, M. Irimia-Vladu, R. Schwödiauer, M. Ullah, H. Sitter, S. Bauer, N. Serdar Sariciftci, L. Leonat, M. Irimia-Vladu, R. Schwödiauer, M. Ullah, H. Sitter, S. Bauer and N. Serdar Sariciftci, *Appl. Phys. Lett.*, **101**, 0233305.
6 E. D. Głowacki, M. Irimia-Vladu, M. Kaltenbrunner, J. Gsiorowski, M. S. White, U. Monkowius, G. Romanazzi, G. P. Suranna, P. Mastrorilli, T. Sekitani, S. Bauer, T. Someya, L. Torsi and N. S. Sariciftci, *Adv. Mater.*, 2013, **25**, 1563-1569.
7 B. M. Schulze, N. T. Shewmon, J. Zhang, D. L. Watkins, J. P. Mudrick, W. Cao, R. Bou Zerdan, A. J. Quartararo, I. Ghiviriga, J. Xue and R. K. Castellano, *J. Mater. Chem. A.* 2014, **2**, 1541-1549.
8 A. Ruiz-Carretero, T. Aytun, C. J. Bruns, C. J. Newcomb, W.-W. Tsai and S. I. Stupp, *J. Mater. Chem. A.*, 2013, **1**, 11674-11681.
9 P. Metrangolo, F. Meyer, T. Pilati, G. Resnati and G. Terraneo, *Angew. Chem. Int. Ed.*, 2008, **47**, 6114-6127.
10 F. Meyer and P. Dubois, *CrystEngComm*, 2013, **15**, 3058-3071.
11 A. Mukherjee, S. Tothadi and G. R. Desiraju, *Acc. Chem. Res.*, 2014, **47**, 2514-2524.
12 D. Cincic, T. Friscic and W. Jones, *New J. Chem.*, 2008, **32**, 1776-1781.
13 P.-T. T. Pham and M. M. Bader, *Cryst. Growth Des.*, 2014, **14**, 916-922.
14 M. Saccone, G. Cavallo, P. Metrangolo, A. Pace, I. Pibiri, T. Pilati, G. Resnati and G. Terraneo, *CrystEngComm*, 2013, **15**, 3102-3105.
15 C. Moussallem, M. Allain, F. Gohier and P. Frere, *New J. Chem.*, 2013, **37**, 409-415.
16 F. Frausto, Z. C. Smith, T. E. Haas and S. W. Thomas Iii, *Chem. Commun.*, 2015, **51**, 8825-8828.
17 P. Politzer, J. S. Murray and T. Clark, *PCCP*, 2013, **15**, 11178-11189.
18 K. Dyduch, M. Mitoraj and A. Michalak, *J. Mol. Model.*, 2013, **19**, 2747-2758.
19 J. Murray, P. Lane, T. Clark, K. Riley and P. Politzer, *J. Mol. Model.*, 2012, **18**, 541-548.
20 C. Präsang, A. C. Whitwood and D. W. Bruce, *Cryst. Growth Des.*, 2009, **9**, 5319-5326.
21 A. Wasilewska, M. Gdaniec and T. Polonski, *CrystEngComm*, 2007, **9**, 203-206.
22 A. D. Becke, *Phys. Rev. A.*, 1988, **38**, 3098-3100.
23 A. D. Becke, *J. Chem. Phys.*, 1993, **98**, 5648-5652.
24 C. Lee, W. Yang and R. G. Parr, *Phys. Rev. B*, 1988, **37**, 785-789.
25 Y. Zhao and D. Truhlar, *Theor. Chem. Acc.*, 2008, **120**, 215-241.
26 D. N. Reinemann, G. S. Tschumper and N. I. Hammer, *ChemPhysChem*, 2014, **15**, 1867-1871.
27 E. C. Constable, C. E. Housecroft, M. Neuburger and C. X. Schmitt, *Polyhedron*, 2006, **25**, 1844-1863.
28 D. Hauchecorne, B. J. van der Veken, A. Moiana and W. A. Herrebout, *Chem. Phys.*, 2010, **374**, 30-36.
29 S. Cherukuvada and T. N. Guru Row, *Cryst. Growth Des.*, 2014, **14**, 4187-4198.
30 N. Schultheiss and A. Newman, *Cryst. Growth Des.,* 2009, **9**, 2950-2967.
31 R. Shannon, *Acta Crystallogr., Sect. A: Found. Crystallogr.*, 1976, **32**, 751-767.
32 A. Bondi, *J. Phys. Chem.*, 1964, **68**, 441-451.
33 D. Feller, *J. Comput. Chem.*, 1996, **17**, 1571-1586.
34 D. Rappoport and F. Furche, *J. Chem. Phys.*, 2010, **133**, 134105.
35 T. H. Dunning, *J. Chem. Phys.*, 1989, **90**, 1007-1023.
36 R. A. Kendall, T. H. Dunning and R. J. Harrison, *J. Chem. Phys.*, 1992, **96**, 6796-6806.

37 D. E. Woon and T. H. Dunning, *J. Chem. Phys*., 1993, **98**, 1358-1371.
38 N. Nagels, D. Hauchecorne and W. Herrebout, *Molecules*, 2013, **18**, 6829-6851.
39 S. Roquet, A. Cravino, P. Leriche, O. Alévêque, P. Frère and J. Roncali, *J. Am. Chem. Soc.*, 2006, **128**, 3459-3466.
40 M. Baldrighi, G. Cavallo, M. R. Chierotti, R. Gobetto, P. Metrangolo, T. Pilati, G. Resnati and G. Terraneo, *Mol. Pharm.*, 2013, **10**, 1760-1772

Synergistic Effects of Halogen Bond and π-π Interactions in Thiophene-based Building Blocks

Jamey Wilson, Jon Steven Dal Williams, Chesney Petkovsek, Peyton Reves, Jonah W. Jurss, Nathan I. Hammer, Gregory Tschumper, Davita L. Watkins*

Department of Chemistry and Biochemistry, University of Mississippi, University, MS 38677-1848

*E-mail: dwatkins@olemiss.edu

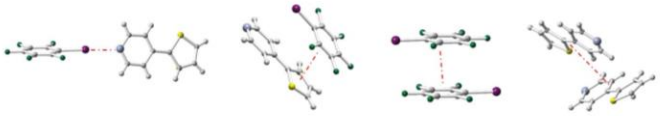

Contacts	Interaction Energy* (kcal/mol)
Halogen Bonding (XB)	-7.2
π-π Stacking (slipped)	-8.6
π-π Stacking $(IPFB)_2$	-5.8
Face to Edge $(Pyr\text{-}T)_2$	-4.4

*Averaged value M06-2X computations with triple-zeta basis sets (6-311+G(2df,2pd), def2-TZVPD and aug-cc-pVTZ); applied Boys-Bernardi couterpoise procedure

The use of a thiophene-based building block (**Pyr-T**) to achieve a supramolecular assembly driven by halogen bonding (XB) is described. X-ray crystallography, NMR, and Raman spectroscopy afford evidence of XB and π-π stacking. Density functional theory (DFT) computations supports experimental observations and reveals that halogen bonding and π stacking provide the dominant energetics in the observed assembly.